Turkish Journal of Physics

http://journals.tubitak.gov.tr/physics/

Research Article

Turk J Phys
(2014) 38: 10 – 16

doi:10.3906/fiz-1305-13

Theoretical investigations of Pt_3X (X = Al, Sc, Hf, Zr) ground state

Adewumi Isaac POPOOLA[1,3,*], **Lesley Heath CHOWN**[2,3], **Lesley Alison CORNISH**[2,3]
[1]Department of Physics, Federal University of Technology Akure, Nigeria
[2]School of Chemical and Metallurgy, University of the Witwatersrand, South Africa
[3]DST/NRF Centre of Excellence in Strong Materials, University of the Witwatersrand, Johannesburg, South Africa

Received: 16.05.2013 • **Accepted:** 22.09.2013 • **Published Online:** 17.01.2014 • **Printed:** 14.02.2014

Abstract: The electronic structure of Pt_3X compounds showed that Pt_3Hf and Pt_3Zr were more stable for the $D0_{24}$ structure, rather than $L1_2$. The compound Pt_3Al was predicted to be the hardest and most ductile, but not with the $L1_2$ structure at ground state. The density of states showed that Pt_3Hf, Pt_3Zr, and Pt_3Al can be stabilized to the $L1_2$ phase with suitable element addition. All calculations were done within the density functional theory framework.

Key words: DFT, hardness, ductile, density of states

1. Introduction

Nickel-based superalloys (NBSAs) are efficient materials that have been used in engines, plants, and production processes since World War II. They traditionally have good elevated temperature strengths and high resistance to oxidation and corrosion [1]. Unfortunately, this class of alloys is presently used near their melting points. For higher system efficiency and less environmental pollution, a new class of alloys with higher melting points is required. To seek a substitute, alloys based on platinum, iridium, and rhodium have been suggested [2–4], primarily because of their fcc structure and higher melting points than nickel. A major drawback with iridium and rhodium alloys is their brittleness [5]. On the other hand, platinum is a recyclable and highly ductile metal [6,7].

The only limitations to the use of platinum are the cost and weight, but these can be reduced by alloying Pt with other metals. An assessment of systems with Pt as the major constituent showed that Pt–Al-based alloys had the highest potential due to precipitation strengthening from Pt_3Al and high oxidation resistance [8]. At high temperature (>1000 °C), Pt_3Al has the $L1_2$ structure [9]. At lower temperatures, there is some uncertainty about the structure of Pt_3Al. The $L1_2$ structure is reported to transform to $tI16$-U_3Si ($D0_c$) structure before another transformation to the $tI16$-Ir_3Si ($D0'_c$) structure [10], while other researchers [11] reported that the low temperature phase was $tP16$-Pt_3Ga type. Both $L1_2$ and $D0_{24}$ structures have been reported in Pt_3Hf and Pt_3Zr [9,12,13], while the structure for Pt_3Sc has been reported to be $L1_2$. All these structure types are shown in Figure 1.

It is now routine to compliment experimental alloy development with theoretical modeling. It not only guides, but can also aid in avoiding the time consuming and expensive "trial and error" approaches that go with traditional material preparation. The fundamental particles that determine the nature of matter are the electrons and nuclei [14]. As the formation of a condensed material involves thousands to millions of atoms,

*Correspondence: ispopoola71@gmail.com

the theory describing these particles is a many-body problem. The intrinsic properties of materials in the large system can be evaluated using a statistical approach. Another strategy for theoretically obtaining material properties relies on approximations that include quantitative theories such as density functional theory (DFT) [15–18].

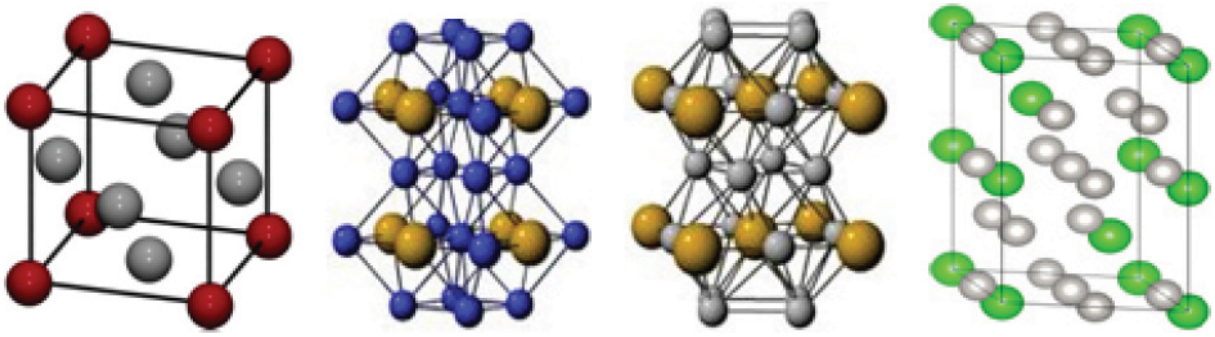

Figure 1. From left to right: $L1_2$, $tP16$-Pt_3Ga, $D0'_c$, and $D0_{24}$ structures. Images from http://cst-www.nrl.navy.mil/lattice//struk/ Accessed May 12, 2012.

The purpose of the present work is to consider the importance of the addition of Al, Sc, Hf, and Zr to Pt in view of the need to achieve low density in the final Pt_3X stoichiometry and their potential use under extreme conditions. Although the present work is theoretical, understanding the ground state structure and mechanical properties of these compounds will add to the knowledge required for the engineering of a new class of high temperature superalloys.

2. Methods

All the calculations are based on the Hohenberg–Kohn [17] and Kohn–Sham [18] DFT formalism. The ground state energy E of a system can be expressed as a function of the density n as:

$$E(n) = T_s(n) + E_H(n) + \mu_{xc}(n) + \int n(r) V_{ext}(r)\, dr \tag{1}$$

In terms of the expansion wave-functions (ψ), the noninteracting kinetic energy $T_s(n)$ is expressed as:

$$T_s(n) = \frac{\hbar^2}{2m} \sum_i \int \psi_i^*(r) \nabla^2 \psi_i(r)\, dr \tag{2}$$

The functional, $\mu_{xc}(n)$, is unknown and is usually approximated. V_{ext} is an external potential energy. The repulsive coulomb interaction between electrons is given by the Hartree energy as:

$$E_H(n) = \int \frac{n(r)\, n(r)}{r - r} dr dr \tag{3}$$

For a many-particle system without any electric or magnetic fields, the external potential in Eq. (1) can be expressed by:

$$||V_{ext}(r) = -\sum_{\alpha=1}^{N} \frac{Z_\alpha}{r - R_\alpha} \tag{4}$$

where N = number of the atoms, Z_α = charge of the $\alpha\,th$ atom, and R_α is the position of the $\alpha\,th$ atom.

The solution of Eq. (1) was achieved with the Vienna Ab-initio Simulation Package (VASP) [19]. VASP is a package for performing quantum mechanical calculations on molecules and solids. It uses an iterative variational method [20] to solve the Kohn–Sham equation of a system. The functional, μ_{xc}, was obtained using the generalized gradient approximation (GGA) [21]. The projector augmented wave method [22] was used during wave-function expansions and "high" precision was sought in the calculation of the kinetic energy. Integration of the Brillouin zones during the self-consistency procedure was performed according to the Monkhorst–Pack scheme [23]. Forces on atoms were less than 0.001 eV/Å during geometrical optimizations. For all the structures considered, the elastic constants, c_{ij}, were calculated using the approach in Mehl et al. [24]. For later use, we define in Eqs. 5–17 the relationship between the bulk modulus, shear modulus, and the elastic constants. In a cubic crystal, 3 elastic constants, namely c_{11}, c_{12}, and c_{44}, are important [25]. According to the Voigt [26] and Reuss [27] approximations, the relationships between the bulk and shear moduli and these elastic constants for cubic structures are:

$$B_V = \frac{c_{11} + 2c_{12}}{3} \tag{5}$$

$$G_V = \frac{c_{11} - c_{12} - 3c_{44}}{5} \tag{6}$$

$$B_R = \frac{c_{11} + 2c_{12}}{3} \tag{7}$$

$$G_R = \frac{5(c_{11} - c_{12})c_{44}}{[4c_{44} + 3\,(c_{11} - c_{12})]}, \tag{8}$$

where B_V and G_V are the bulk and shear moduli as defined by the Voigt notation and B_R and G_R are the bulk and shear moduli according to the Reuss notation.

For a tetragonal lattice:

$$B_V = \frac{1}{9}(2c_{11} + c_{12}) + c_{33} + 4c_{13} \tag{9}$$

$$G_V = \frac{1}{30}(M + 3c_{11} - 3c_{12} + 12c_{44} + 6c_{66}), \tag{10}$$

where

$$M = c_{11} + c_{12} + 2c_{33} - 4c_{13} \tag{11}$$

and the Reuss bounds are:

$$B_R = \frac{C^2}{M} \tag{12}$$

$$G_R = 15\left[\left(\frac{18B_V}{C^2}\right) + \left(\frac{6}{c_{11} - c_{12}}\right) + \frac{6}{c_{44}} + \frac{3}{c_{66}}\right]^{-1}, \tag{13}$$

where

$$C^2 = (c_{11} + c_{12})c_{33} - 2c_{13}^2. \tag{14}$$

In this study, the averages between the Voigt and Reuss bounds (Hill averages) for all the crystals considered were obtained by:

$$B = \frac{1}{2}(B_V + B_R) \tag{15}$$

$$G = \frac{1}{2}(G_V + G_R) \tag{16}$$

The Poisson's ratio (v) was calculated from the relation:

$$v = \frac{3B - 2G}{2(3B + G)} \tag{17}$$

3. Results

3.1. Phase stability and mechanical properties

The results of the calculations are given in the Table. Based on the equilibrium energy E_0 data, the most stable compound was $D0_{24}$-Pt_3Hf. Because of its lowest E_0 value, the $D0_{24}$ structure will be more readily formed in Pt_3Hf by thermodynamic means than the $L1_2$ structure. At ground state, both Pt_3Hf and Pt_3Zr are more stable in the $D0_{24}$ phase than in the $L1_2$ phase. The Pt_3Al compound is predicted to be more stable in the $tP16$-Pt_3Ga structure than in the $L1_2$ structures.

As the hardness of a crystal relates to the bulk modulus [28–30], the hardest compound according to the results was Pt_3Al in the $tP16$-Pt_3Ga structure. The least hard compound was $D0_{24}$-Pt_3Hf. $D0_{24}$-Pt_3Zr is predicted to be harder than $D0_{24}$-Pt3Hf, and the available experimental data [31] showed that the Vickers microhardness of $D0_{24}$-Pt_3Hf and $D0_{24}$-Pt_3Zr is 796 HV and 811 HV, respectively. With regards to their densities, Pt_3Al and Pt_3Sc are less dense compared with Pt_3Hf and Pt_3Zr. According to the Pugh criterion [32], a ductile compound should have a B/G $>$1.75. The results showed that $D0_{24}$-Pt_3Hf is brittle, while the other compounds are predicted to be ductile, with Pt_3Al ($tP16$-Pt_3Ga type) being the most ductile compound.

3.2. Density of states

The density of states (DOS) of a system describes the number of states per energy interval at each energy level that are available for occupation by electrons. When a compound is formed, electron redistribution occurs, creating different types of electronic structures. The correlations between the electronic structure of a material and its various physical properties are important, and, in some cases, can be used to predict new structures [33–35]. The DOS for all the phases in the Table are given in Figures 2a–2d.

The DOS plots further confirmed that the structures of Pt_3Al, Pt_3Hf, and Pt_3Zr will not be $L1_2$ or $D0'_c$. For $L1_2$-Pt_3Al, the Fermi level falls on the antibonding (increasing energy) part of the spectrum—an indication of a metastable phase. The Fermi level on the DOS of $D0'_c$-Pt_3Al was on a peak, which indicates an unstable phase. The Fermi level on the DOS of Pt_3Al ($tP16$-Pt_3Ga type) was on a plateau, showing that this is the most stable of all the structures ever reported for Pt_3Al.

The Fermi levels on the DOS of both $D0_{24}$-Pt_3Hf and $L1_2$-Pt_3Hf were on the pseudogap.

Moreover, the Fermi level of $D0_{24}$-Pt_3Hf was more on the nonbonding (reducing energy) part of the spectrum and this phase is predicted to be more stable than the $L1_2$-Pt_3Hf phase that had its Fermi level more on the antibonding (increasing energy) side of the DOS spectrum. Likewise, $D0_{24}$-Pt_3Zr is predicted to be more stable than $L1_2$-Pt_3Zr. The DOS spectrum of $D0_{24}$-Pt_3Zr had its Fermi level exactly on the pseudogap, while that of $L1_2$-Pt_3Zr was on the antibonding side of the DOS spectrum. At ground state, therefore, the phases will be $D0_{24}$ for Pt_3Hf and Pt_3Zr and $tP16$-Pt_3Ga for Pt_3Al, agreeing with previous works [31,38].

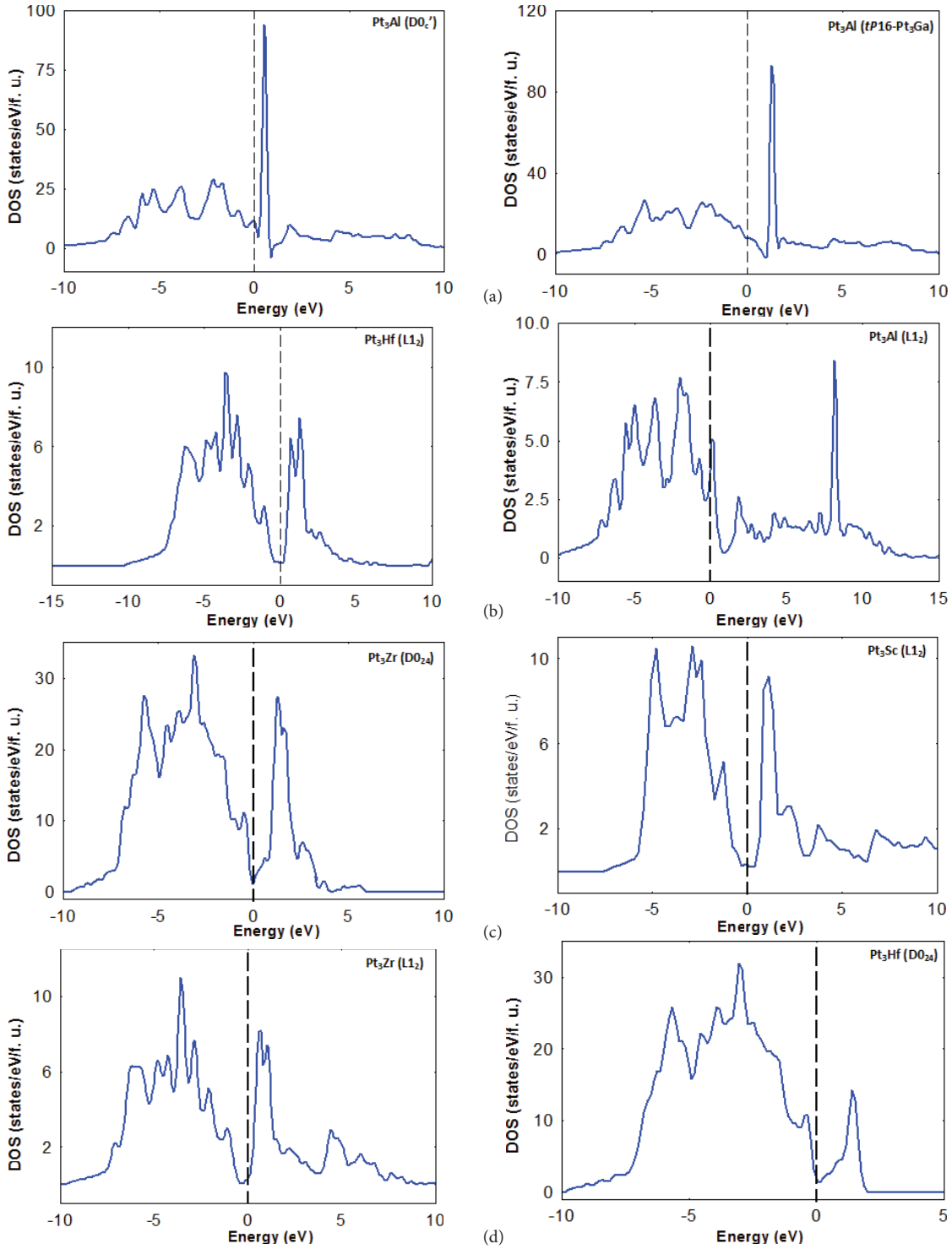

Figure 2. a) Total electronic density of states for Pt_3Al in $D0_c$' and $tP16$-Pt_3Ga structures. Energies relative to Fermi level are indicated by the dotted vertical line. b) Total electronic density of states for Pt_3Al and Pt_3Hf in the $L1_2$ structures. Energies relative to Fermi level are indicated by the dotted vertical line. c) Total electronic density of states for Pt_3Zr ($D0_{24}$) and $L1_2$-Pt3Sc structures. Energies relative to Fermi level are indicated by the dotted vertical line. d) Total electronic density of states for structures of Pt_3Zr ($L1_2$) and Pt_3Hf ($D0_{24}$). Energies relative to Fermi level are indicated by the dotted vertical line.

Table. Calculated bulk modulus (B), shear modulus (G), B/G ratio, Poisson's ratio (v), equilibrium energy (E_0), and density (ρ^{cal}) for Pt_3X compounds. Experimental data are in brackets and all moduli are in GPa.

Compound	Structure	B	G	B/G	v	E_0 (eV/at.)	ρ^{cal}(g.cm^{-3})	Ref.
Pt_3Sc	$L1_2$	250	103	2.43	0.29	–7.178	12.36	-
	$L1_2$	280	108	2.59	0.30	–6.256	12.24	-
Pt_3Al	$D0'_c$	309	98	3.15	0.30	–6.297	12.68	-
	Pt_3Ga	378	71	5.32	0.34	–6.354	12.68	-
	$L1_2$	290	120	2.42	0.28	–8.129	18.88	-
Pt_3Hf	$D0_{24}$	151	111	1.36	0.31	–8.135	19.59 [19.62]	31
	$L1_2$	282	113	2.50	0.29	–7.693	14.31	
Pt_3Zr	$D0_{24}$	280	106	2.64	0.31	–7.701	16.96 [18.13]	36,37

However, the results in the Table showed that Pt_3Hf and Pt_3Zr had higher hardness (indicated by B) and lower density in the $L1_2$ structure than in the $D0_{24}$ phase. Moreover, the ductility was much better in the $L1_2$ structure. An assessment of the DOS plots showed that for these compounds to exist in the $L1_2$ structures, energy reduction in the system is important, and this can be achieved by the addition of low electron elements. The DOS results also showed that an additional element will be required to attain a more stable structure for $L1_2$-Pt_3Al. In this case, however, elements with many electrons such as palladium, cobalt, and chromium are predicted to play a beneficial role. The Fermi level is far from the pseudogap; therefore, more electrons are required to shift the Fermi level to the pseudogap.

4. Conclusions

Both the elastic and electronic structure properties of platinum alloys in the stoichiometry Pt_3X (X = Al, Sc, Hf, Zr) were evaluated within the framework of DFT. The most stable compound was $D0_{24}$-Pt_3Hf. The compressibility of the compounds was in the order of $D0_{24}$-Pt_3Hf >L12-Pt_3Sc >$L1_2$-Pt_3Al/ $D0_{24}$-Pt_3Zr >$L1_2$-Pt_3Zr >$L1_2$-Pt_3Hf >$D0'_c$-Pt_3Al >Pt_3Al ($tP16$- Pt_3Ga). Except for $D0_{24}$-Pt_3Hf, all compounds are predicted to be ductile. Pt_3Al had the highest potential on the account of hardness, ductility, and density. The DOS showed that additional elements will be required to obtain Pt_3Al, Pt_3Hf, and Pt_3Zr as $L1_2$ structures at ground state.

Acknowledgments

We acknowledge support from the Department of Science and Technology, and National

Research Foundation, South Africa, and African Materials Science and Engineering Network (AMSEN - a Carnegie-RISE Network). We profoundly thank Prof JE Lowther and Prof IA Fuwape for useful discussions.

References

[1] Sims, C. T.; Stoloff, N. S.; Hagel, W. C. (Eds.) *Superalloys II*; Wiley Inter-Science: New York, NY, USA, 1987.

[2] Yamabe-Mitarai, Y.; Koizumi, Y.; Murakami, H.; Ro, Y.; Maruko, T.; Harada, H. *Scripta Mater.* **1996**, *35*, 211–215.

[3] Cornish, L. A.; Fischer, B.; Völkl, R. *MRS Bulletin* **2003**, *28*.

[4] Wolf, I. M.; Hill, P. J. *Plat. Met. Rev.* **2000**, *44*, 158–165.

[5] Panfilov, P.; Yermarkov, A.; Dmitriev, V.; Timofeev, N. *Plat. Met. Rev.* **1991**, *35*, 196–200.

[6] Vaccaro, J. *Materials Handbook*; McGraw-Hill: New York, NY, USA, 2002.

[7] Schwartz, M. *CRC Encyclopedia of Materials Parts and Finish*; CRC Press: Boca Raton, FL, USA, 2002.

[8] Hill, P. J.; Cornish, L. A.; Witcomb, M. J.; Wolf, I. M. *Proc. Int. Symp. on High Temperature Corrosion and Protection*: Science Reviews, Japan, 2000.

[9] Massalski, T. B., Ed.; *Binary Alloy Phase Diagrams*: ASM International, Ohio, USA, 1990.

[10] Oya, Y.; Mishima, U.; Suzuki, T. *Z. Metallkde* **1987**, *78*, 485–490.

[11] McAlister, A.J.; Kahan, D.J. *Bull. Alloy Phase Diagr.* **1986**, *7*, 47–51.

[12] Schubert, K.; Bhan, S.; Biswas, T. K.; Frank, K.; Pandy, P. K. *Naturwisenchaften* **1968**, *55*.

[13] Wallbaum, H. J. *Naturwisenchaften* **1943**, *31*.

[14] Martin, R. M. *Electronic Structure, Basic Theory and Practical Methods*: Cambridge University Press, Cambridge, UK, 2004.

[15] Thomas, L. H. *Proceedings of Cambridge Philosophical Society*, **1927** *23*, 542–548.

[16] Fermi, E. *Zeitschrift Fur Physik* **1928**, *43*, 73.

[17] Hohenberg P.; Kohn, W. *Phys. Rev. B* **1964**, *136*, 864–871.

[18] Kohn, W.; Sham, L. J. *Phys. Rev. A* **1965**, *140*, 1133–1138.

[19] Kresse, G.; Furthmüller, J. *Comp. Mat. Sci.* **1996**, *6*, 15–50.

[20] Car, R.; Parrinello, M. *Phys. Rev. Lett.* **1985**, 55, 2471–2474.

[21] Perdew, J.P.; Burke, K.; Ernzerhof, M. *Phys. Rev. Lett.* **1996**, *77*, 3865–3868.

[22] BlÖchl, P.E. *Phys. Rev. B* 1994, *50*, 17953–17979.

[23] Monkhorst, H. J.; Pack, J. D. *Phys. Rev. B* **1976**, *13*, 5188–5192.

[24] Mehl, M. J.; Osburn, J. E.; Papacostantopoulos, D.A.; Klein, B. M. *Phys. Rev. B* **1990**, *41*, 10311–10323.

[25] Nye, J. F. *Physical Properties of Crystals*: Clarendon, Oxford, UK, 1960.

[26] Voigt, W. *Lehrbuch der Kristallphysik*: *Teuibner Leipzig* **1928**, 830–831.

[27] Reuss, A. *Z. Angew. Math. Mech.* **1929**, *9*, 49–58.

[28] Goble, R. J.; Scott, S. D. *Canadian Minerologist* **1985**, *23*, 273–285.

[29] Liu, A. Y.; Cohen, M. L. *Science* **1989**, *245*, 841–842.

[30] Leger, J. M.; Haines, J.; Schmidt, M.; Petitet, J. P.; Pereira, A. S.; Dajornada, J. A. H. *Nature* **1996**, *383*, 401.

[31] Pecora, L. M.; Ficalora, P. J. *Journal of Electronic Materials* **1977**, *6*, 531–540.

[32] Pugh, S. F. *Philos. Mag.* **1954**, *45*, 823–843.

[33] Gelatt, C. D.; Williams, A. R. (Jr.); Moruzzi, V. L. *Phys. Rev. B* **1983**, *27*, 2005–2013.

[34] Pastural, A.; Colinet, C.; Hitter, P. *Physica B* **1985**, *132*, 177.

[35] Ravindran, P.; Asokamani, R. *Bull. Mater. Sci.* **1997**, *20*, 613–622.

[36] Simmons, G.; Wang, H. *A Handbook of Single Crystal Elastic Constants and Calculated Aggregate Properties*: MIT Press, Cambridge, MA, USA, 1971.

[37] Upadhya, K.; Yang, J. M.; Hoffman, W. Advanced Materials for Ultrahigh Temperature Structural Applications above 2000 °C. www.dtic.mil. Accessed August 25, 2012.

[38] Völkl, R.; Yamabe-Mitarai, Y.; Huan, C.; Harada, H. *Metall. and Mater. Trans. A* **2005**, *36*, 2881–2892.